

Effect of boundary slip on electroosmotic flow in a curved rectangular microchannel

Yong-Bo Liu(刘勇波)1,2,

Citation: Chin. Phys. B, 2024, 33 (**7**): 074101. DOI: 10.1088/1674-1056/ad3340
Journal homepage: http://cpb.iphy.ac.cn; http://iopscience.iop.org/cpb

What follows is a list of articles you may be interested in

Electric field and force characteristic of dust aerosol particles on the surface of high-voltage transmission line

Yingge Liu(刘滢格), Xingcai Li(李兴财), Juan Wang(王娟), Xin Ma(马鑫), and Wenhai Sun(孙文海)
Chin. Phys. B, 2024, 33 (**1**): 014101. DOI: 10.1088/1674-1056/ad0140

Electrostatic force of dust deposition originating from contact between particles and photovoltaic glass

Xing-Cai Li(李兴财), Juan Wang(王娟), and Guo-Qing Su(苏国庆)
Chin. Phys. B, 2021, 30 (**10**): 104101. DOI: 10.1088/1674-1056/abeb12

Effect of patterned hydrodynamic slip on electromagnetohydrodynamic flow in parallel plate microchannel

Chun-Hong Yang(杨春红) and Yong-Jun Jian(菅永军)
Chin. Phys. B, 2020, 29 (**11**): 114101. DOI: 10.1088/1674-1056/abab71

Uniform stable conformal convolutional perfectly matched layer for enlarged cell technique conformal finite-difference time-domain method

Wang Yue (王玥), Wang Jian-Guo (王建国), Chen Zai-Gao (陈再高)
Chin. Phys. B, 2015, 24 (**2**): 024101. DOI: 10.1088/1674-1056/24/2/024101

Effect of boundary slip on electroosmotic flow in a curved rectangular microchannel

Yong-Bo Liu(刘勇波)[1,2,†]

[1] *College of Mathematics Science, Inner Mongolia Normal University, Hohhot* 010022, *China*
[2] *Inner Mongolia Center for Applied Mathematics, Hohhot* 010022, *China*

(Received 18 October 2023; revised manuscript received 26 February 2024; accepted manuscript online 13 March 2024)

The aim of this study is to numerically investigate the impact of boundary slip on electroosmotic flow (EOF) in curved rectangular microchannels. Navier slip boundary conditions were employed at the curved microchannel walls. The electric potential distribution was governed by the Poisson–Boltzmann equation, whereas the velocity distribution was determined by the Navier–Stokes equation. The finite-difference method was employed to solve these two equations. The detailed discussion focuses on the impact of the curvature ratio, electrokinetic width, aspect ratio and slip length on the velocity. The results indicate that the present problem is strongly dependent on these parameters. The results demonstrate that by varying the dimensionless slip length from 0.001 to 0.01 while maintaining a curvature ratio of 0.5 there is a twofold increase in the maximum velocity. Moreover, this increase becomes more pronounced at higher curvature ratios. In addition, the velocity difference between the inner and outer radial regions increases with increasing slip length. Therefore, the incorporation of the slip boundary condition results in an augmented velocity and a more non-uniform velocity distribution. The findings presented here offer valuable insights into the design and optimization of EOF performance in curved hydrophobic microchannels featuring rectangular cross-sections.

Keywords: electroosmotic flow (EOF), curved rectangular microchannels, slip boundary conditions

PACS: 41.20.Cv, 47.10.ad, 47.61.–k **DOI:** 10.1088/1674-1056/ad3340

1. Introduction

In recent decades, numerous researchers have delved into the realm of microscale transport phenomena because of their wide-ranging applications in micromixers,[1] chemical analysis,[2] biological analysis,[3] drug delivery,[4] DNA analysis,[5] heat transfer,[6] etc. In microchannels, liquid flow is driven primarily by pressure gradients,[7] electric fields[8] and electromagnetic fields.[9] Among these, electric-field-driven electroosmotic flow (EOF) has garnered significant attention owing to its advantages such as precise flow control, plug-like flow and simple fabrication processes.

In 1852, Wiedemann[10] established a basic theory of EOF in microchannels based on numerous experiments; the rationality of this theory has been extensively proven many times by scientists. Since then, numerous scholars have conducted theoretical and experimental investigations on EOF in various types of microchannels, such as parallel-plate microchannels,[11] rectangular microchannels,[12] semicircular microchannels[13] and microannuli,[14] among others.

Although all the investigations mentioned above involved straight microchannels, the significance of fluid flow in curved microchannels has also been demonstrated. Microfluidic devices such as micromixers,[15] microseparators[16] and microreactors[17] often consist of curved microchannels. In addition, curved microchannels have the advantages of increasing heat transfer,[18] enhancing mixing efficiency,[19] changing the flow direction and increasing the effective channel length. Therefore, investigations of EOF in curved microchannels are necessary. In 2004, Luo first explored transient EOF in a curved microtube with a rectangular cross section.[20] Luo's team further studied the EOF in curved rectangular microchannels by considering secondary flows.[21,22] The investigations conducted in Refs. [20–22] primarily focused on the start-up process of fluid flow in curved microchannels, specifically addressing the transition from a state of rest to a state of steady flow. However, understanding the characteristics of fully developed EOF within curved microchannels is another essential issue. Lu *et al.*[23] developed a precise model to investigate the influence of curvature on fully developed EOF and heat transfer in a corrugated curved microtube. Their study focused on two-dimensional flows due to the roughness of the pipe walls. Salahuddin *et al.*[24] conducted another investigation in a corrugated curved microtube, primarily focusing on the peristaltic EOF of a nanofluid. In a recently published study[25] we investigated the heat transfer and entropy generation of EOF in a curved rectangular nanochannel at high zeta potentials, with consideration of the influence of steric effects. Previous studies on EOF in curved rectangular ducts have primarily focused on Newtonian fluids. However, non-Newtonian fluids, such as protein solutions, polymeric solutions and blood samples, are often manipulated in microchannels. Therefore, investigations of the influence of non-Newtonian effects on EOF through curved mi-

[†]Corresponding author. E-mail: liuyb@mail.imu.edu.cn
© 2024 Chinese Physical Society and IOP Publishing Ltd

crochannels are also necessary. The constitutive equations of non-Newtonian fluids differ significantly from those of Newtonian fluids, resulting in a lack of consistency in the momentum equations satisfied by the velocities, and thus leading to distinct velocity distributions. Recently, Nekoubin[26] investigated the effect of power-law fluids and high zeta potential conditions on EOF in curved microchannels. Narla and Tripathi[27] developed a mathematical model for blood flow in curved microvessels. The heat and mass transfer of EOF in a curved channel was investigated by Kolsi *et al.*[28] using a viscoelastic nanofluid as the working fluid. The entropy generation of the EOF of a Williamson fluid in a curved microchannel was investigated by Khan *et al.*[29] Most recently, Si *et al.*[30] investigated the periodic EOF of Oldroyd-B fluids in a curved rectangular microchannel by considering the effect of secondary flow. Yang *et al.*[31] made another significant contribution to the study of EOF in curved microchannels using Maxwell fluids.

The presence of surface effects in microchannels and nanochannels is crucial for fluid flow, and the significance of interfacial slip cannot be overlooked.[32] Additionally, the use of a hydrophobic surface can increase the volume flow rate, which is beneficial in practical applications of EOF. Thus, numerous researchers have contributed to the investigation of EOF in hydrophobic microchannels through consideration of the slip boundary conditions. Goswami *et al.*[33] investigated the EOF behavior of a Powell–Eyring fluid by incorporating the Navier slip boundary condition and observed an amplification in the volumetric flow rate due to the presence of slip conditions. The EOF of a two-layer fluid in a hydrophobic microchannel was investigated by Shit *et al.*,[34] who considered the influence of wall slip effects on the flow. A study conducted by Majhi *et al.*[35] demonstrated that the enhancement of EOF in hydrophobic structured microchannels with nozzle-diffuser configurations could be attributed to the boundary slip phenomenon occurring within these channels. By considering the combined influence of ion size and slip effects, Sujith *et al.*[36] developed a theoretical model for EOF and entropy generation in a hydrophobic microchannel. The slip length in hydrophobic microchannels is another important factor that can enhance the zeta potential, thereby influencing the estimation of the electroosmotic velocity. Recently, considering slip-dependent zeta potentials, several scholars have investigated the EOF of various fluids, including Newtonian fluids,[37–39] Phan–Thien–Tanner fluids,[40] generalized Maxwell fluids,[41,42] power-law fluids[43] and two immiscible fluids.[44]

As previously mentioned, although EOF in curved microchannels may offer certain advantages in terms of heat transfer and mixing, this essential problem has not yet received sufficient attention, especially for flow in a curved hydrophobic microchannel. Existing studies on EOF have investigated either the flow in curved microchannels with no-slip boundary conditions or the flow in straight microchannels with slip boundary conditions. In other words, the characteristics of EOF in a hydrophobic microchannel with curved geometry remain unclear. The EOF in curved rectangular microchannels exhibits distinct characteristics compared with those in straight rectangular microchannels, primarily because of the influence of the curvature effect. Moreover, instead of employing a constant electric field as used in straight rectangular microchannels, a constant electric potential is applied along the axis in curved microchannels. These two differences ultimately lead to a unique velocity distribution for EOF in curved microchannels. The application of a constant external electric potential induces varying electric field forces on the fluid in different regions of the channel, leading to a more non-uniform velocity distribution. Additionally, despite the contributions of numerous researchers to the investigation of EOF in hydrophobic microchannels,[33–44] almost all studies on EOF in rectangular microchannels have predominantly employed no-slip boundary conditions, even in straight rectangular microchannels. Accordingly, the present study numerically investigates the creeping Dean EOF in curved rectangular microchannels with slip boundary conditions for the first time. The incorporation of slip boundary conditions may result in different velocities and velocity distributions. However, the combined influence of slip length and curvature effect on EOF in curved microchannels remains unexplored. The heat transfer behavior in microchannels associated with EOF is influenced by both the velocity and the velocity distribution. Therefore, the present study investigates the combined effects of boundary slip and curvature on EOF, which holds potential for future investigations into heat transfer characteristics in such flows. The centripetal force can be neglected in the case of the creeping Dean flow considered herein because of the typically low EOF velocity in the microchannels. In other words, the lateral components of the velocity can be disregarded compared with the magnitude of the main velocity. Consequently, this can be regarded as a one-dimensional problem. The present study focuses on investigating steady EOF in a curved microchannel with the aim of facilitating precise control of the EOF velocity. The remainder of this paper is organized as follows. In Section 2, the dimensionless governing equations and corresponding boundary conditions for the electric potential and velocity are derived and solved numerically using the finite-difference method. The validity of our results is verified in Section 3 by comparing them with other reported findings, demonstrating remarkable consistency. Furthermore, we delve into the details of the dependence of the velocity distribution and average velocity on the corresponding dimensionless physical parameters based on the

actual parameter values. Section 4 presents our intriguing conclusions. Appendix A provides a detailed presentation of the finite-difference schemes for the governing equations of electric potential and velocity.

2. Theoretical modeling

In this section, we present the mathematical modeling of a fully developed EOF through a curved hydrophobic microchannel with a rectangular cross-section, in which the effect of slip length on velocity is considered. The fluid is assumed to be an incompressible Newtonian fluid. The flow is considered to be a creeping Dean flow, thereby reducing the present problem to a one-dimensional problem. To analyze the flow field, we set up a cylindrical coordinate system (r^*, θ^*, z^*), as shown in Fig. 1. The width and height are a^* and b^*, respectively. $r^* = r_{\rm i}^*$ and $r^* = r_{\rm o}^*$ represent the inner and outer walls, respectively, and $R^* = (r_{\rm i}^* + r_{\rm o}^*)/2$ is the radius of curvature of the curved microchannel. The surface zeta potential ζ^* is applied to the four channel walls. The applied electric potential is denoted by φ^*.

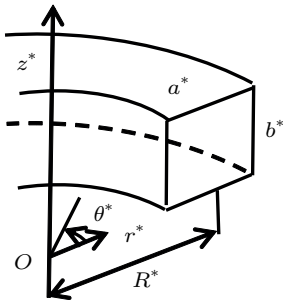


Fig. 1. The curved microchannel.

2.1. The electrical potential equation and its boundary conditions

Prior to analyzing the EOF velocity in a curved rectangular microchannel, the corresponding electrical potential distribution in the electric double layer should first be given. It is governed by the following Poisson–Boltzmann equation:[43]

$$\nabla^2 \psi = K^2 \sinh(\psi), \tag{1}$$

where $\psi = \psi^*/\psi_{\rm ref}$ is the dimensionless electrical potential, $\psi_{\rm ref} = k_{\rm B}T_0/(eZ)$ is the characteristic electrical potential, e is the elementary charge, Z is the valence of the cations, $k_{\rm B}$ is the Boltzmann constant, T_0 is the room temperature, $K = \kappa R_{\rm h}$ is the electrokinetic width, $\kappa = (2n_0e^2Z^2/(\varepsilon k_{\rm B}T_0))^{1/2}$ is the Debye–Hückel parameter, $R_{\rm h} = 2a^*b^*/(a^*+b^*)$ is the hydraulic diameter, ε is the dielectric constant and n_0 is the ion density of the bulk liquid. For the fully developed EOF considered here, the partial derivative of the variable ψ with respect to θ is zero. Thus, Eq. (1) can be reformulated as follows:

$$\frac{\partial^2\psi}{\partial r^2} + \frac{1}{r}\frac{\partial\psi}{\partial r} + \frac{\partial^2\psi}{\partial z^2} = K^2\sinh(\psi), \tag{2}$$

where $r = r^*/R_{\rm h}$ and $z = z^*/R_{\rm h}$ are the dimensionless coordinates. The dimensionless boundary conditions corresponding to Eq. (1) are expressed as follows:

$$\psi|_{r=r_{\rm i}} = \zeta, \quad \psi|_{r=r_{\rm o}} = \zeta, \quad \psi|_{z=0} = \zeta, \quad \psi|_{z=b} = \zeta, \tag{3}$$

where $r_{\rm i} = r_{\rm i}^*/R_{\rm h}$, $r_{\rm o} = r_{\rm o}^*/R_{\rm h}$, $b = b^*/R_{\rm h}$, and $\zeta = \zeta^*/\psi_{\rm ref}$ are normalized parameters.

2.2. The velocity equation and its boundary conditions

Subsequently, the velocity distribution was analyzed. Because of the extremely low EOF velocity in microchannels, the EOF in this study is considered to be a creeping Dean flow and only along the θ^*-direction (for details, please see Ref. [45]). Therefore, for a fully developed EOF in curved rectangular microchannels, considering the electric field force, the one-dimensional Navier–Stokes equation is expressed as[45]

$$\mu\left(\frac{\partial^2 v_{\theta^*}}{\partial r^{*2}} + \frac{1}{r^*}\frac{\partial v_{\theta^*}}{\partial r^*} - \frac{v_{\theta^*}}{r^{*2}} + \frac{\partial^2 v_{\theta^*}}{\partial z^{*2}}\right) + \rho_{\rm e}E^* = 0, \tag{4}$$

where μ represents the fluid viscosity, $v_{\theta*}$ represents the velocity component along the θ^* direction, $\rho_{\rm e}$ is the net charge density expressed as[46]

$$\rho_{\rm e} = -2eZn_0\sinh\left(\frac{eZ\psi^*}{k_{\rm B}T_0}\right), \tag{5}$$

and E^* represents the electric field, which is determined by taking the partial derivative of the applied electric potential φ^*[26]

$$E^* = -\frac{1}{r^*}\frac{\partial\phi^*}{\partial\theta^*}. \tag{6}$$

The electric field at the center of the channel ($r^* = R^*$) is assumed to be a constant, expressed as

$$E_0^* = -\frac{1}{R^*}\frac{\partial\phi^*}{\partial\theta^*} = \text{constant}. \tag{7}$$

Substituting Eq. (5)–(7) into Eq. (4),

$$\mu\left(\frac{\partial^2 v_{\theta^*}}{\partial r^{*2}} + \frac{1}{r^*}\frac{\partial v_{\theta^*}}{\partial r^*} - \frac{v_{\theta^*}}{r^{*2}} + \frac{\partial^2 v_{\theta^*}}{\partial z^{*2}}\right) - 2eZn_0\sinh\left(\frac{eZ\psi^*}{k_{\rm B}T_0}\right)\frac{R^*}{r^*}E_0^* = 0. \tag{8}$$

Then, the following Navier slip boundary conditions are imposed at the channel walls:[35]

$$v_{\theta^*}|_{r^*=r_{\rm i}^*} = \beta^*\left.\frac{\partial v_{\theta^*}}{\partial r^*}\right|_{r^*=r_{\rm i}^*}, \quad v_{\theta^*}|_{r^*=r_{\rm o}^*} = -\beta^*\left.\frac{\partial v_{\theta^*}}{\partial r^*}\right|_{r^*=r_{\rm o}^*},$$
$$v_{\theta^*}|_{z^*=0} = \beta^*\left.\frac{\partial v_{\theta^*}}{\partial z^*}\right|_{z^*=0}, \quad v_{\theta^*}|_{z^*=b^*} = -\beta^*\left.\frac{\partial v_{\theta^*}}{\partial z^*}\right|_{z^*=b^*}. \tag{9}$$

In Eq. (9), β^* represents the slip length of the microchannel. Some non-dimensional parameters are imposed to simplify the analysis

$$u = \frac{v_{\theta^*}}{u^*}, \quad u^* = \frac{\varepsilon k_{\rm B}T_0E_0^*}{\mu eZ}, \quad R = \frac{R^*}{R_{\rm h}},$$

$$\delta = \frac{a}{2R}, \quad A_{\mathrm{R}} = \frac{a}{b}, \quad \beta = \frac{\beta^*}{R_{\mathrm{h}}}. \tag{10}$$

Here, u^* is the characteristic velocity, δ is the curvature ratio, β is the dimensionless slip length and A_{R} is the aspect ratio. By substituting the non-dimensional parameters defined above into Eqs. (8) and (9), the following dimensionless equation and boundary conditions are obtained:

$$\frac{\partial^2 u}{\partial r^2} + \frac{1}{r}\frac{\partial u}{\partial r} - \frac{u}{r^2} + \frac{\partial^2 u}{\partial z^2} - K^2 \sinh(\psi)\frac{R}{r} = 0, \tag{11}$$

$$u|_{r=r_{\mathrm{i}}} = \beta \left.\frac{\partial u}{\partial r}\right|_{r=r_{\mathrm{i}}}, \quad u|_{r=r_{\mathrm{o}}} = -\beta \left.\frac{\partial u}{\partial r}\right|_{r=r_{\mathrm{o}}},$$

$$u|_{z=0} = \beta \left.\frac{\partial u}{\partial z}\right|_{z=0}, \quad u|_{z=b} = -\beta \left.\frac{\partial u}{\partial z}\right|_{z=b}, \tag{12}$$

where

$$r_{\mathrm{i}} = \frac{1}{4}\left(\frac{1}{\delta} - 1\right)(1 + A_{\mathrm{R}}), \quad r_{\mathrm{o}} = \frac{1}{4}\left(\frac{1}{\delta} + 1\right)(1 + A_{\mathrm{R}}),$$

$$b = \frac{1}{2}\left(1 + \frac{1}{A_{\mathrm{R}}}\right), \quad R = \frac{1}{4\delta}(1 + A_{\mathrm{R}}). \tag{13}$$

The dimensionless average velocity Q can be obtained using the following expression:

$$Q = \frac{Q^*}{u^*} = \frac{1}{ab}\int_{r_{\mathrm{i}}}^{r_{\mathrm{o}}}\int_0^b u(r,z)\,\mathrm{d}z\,\mathrm{d}r. \tag{14}$$

Here, Q^* is the average velocity across the rectangular cross-section.

2.3. Numerical solutions for the electrical potential and velocity

The numerical solutions for the governing equations of the electrical potential (Eq. (2)) and velocity (Eq. (11)) under the boundary conditions (Eqs. (3) and (12), respectively) were obtained using the finite-difference method. Subsequently, a solution for the average velocity Q was obtained. Appendix A presents the corresponding difference schemes. The discretized system of the above equations was solved using Gaussian elimination.[47] The solution was iteratively solved starting from zero until the maximum relative error met the predetermined convergence criterion, which is set to 10^{-6}.

3. Results and discussion

In this section, to validate the accuracy of the obtained results, the solution for the velocity is compared with the existing experimental data for the special case. The dimensionless velocity and average velocity are heavily influenced by the dimensionless slip length β, curvature ratio of the curved channel δ, aspect ratio A_{R} and electrokinetic width K. Hence, we present the ranges of the aforementioned parameters based on actual physical scenarios. Typically, the following parametric values are used:[48–51] $e = 1.6 \times 10^{-19}$ C, $\rho = 10^3$ kg·m^{-3}, $k_{\mathrm{B}} = 1.38 \times 10^{-23}$ J·K^{-1}, $\varepsilon = 6.95 \times 10^{-10}$ C^2·J^{-1}·m^{-1}, $\mu = 10^{-3}$ kg·m^{-1}·s^{-1}, $T_0 = 298$ K and $Z = 1$. For a typical microchannel, the hydraulic diameter R_{h} is set to 10^{-5} m.[37] Based on the data reported in previous studies,[37,39,51] it can be inferred that the slip length β^* is less than 10^{-7} m. Thus, the dimensionless slip length β remains up to 0.01 as per the expression $\beta = \beta^*/R_{\mathrm{h}}$. For the high zeta potential under consideration, the value of the dimensionless zeta potential ζ was varied from -3 to -1. The curvature ratio of the curved channel δ was varied from 0.2 to 0.8.[50] The aspect ratio A_{R} is assumed to be 1 in the subsequent analysis, unless otherwise specified. The electrolyte concentration was varied from 10^{-7} M to 10^{-5} M, resulting in variation of the electrokinetic width K from 10 to 100.

In Fig. 2, the results of the present average velocity are compared with the experimental results reported by Wang *et al.*,[52] who studied EOF in a straight rectangular microchannel. The dimensionless slip length β of the present model was assumed to be zero for the purpose of conducting a comparative analysis under identical conditions. In addition, the curvature ratio δ was set to an exceedingly minute value of 0.01, thereby allowing the curved microchannel to be regarded as straight. The values of the other parameters were $a^* = 10^{-4}$ m, $b^* = 10^{-4}$ m, ion concentration $c_0 = 10^{-3}$ M and $\zeta^* = 0.0575$ V. It can be clearly observed from Fig. 2 that the present results agree very well with the previous experimental results. This comparison thoroughly confirms the accuracy of our proposed model.

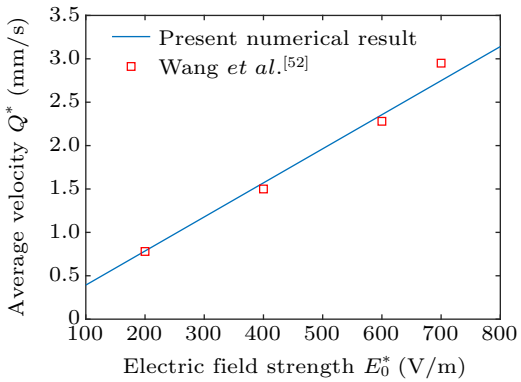


Fig. 2. Comparison of the current average velocity results with the experimental findings of Wang *et al.*[52] for $a^* = 10^{-4}$ m, $b^* = 10^{-4}$ m, $\zeta^* = 0.0575$ V and an NaCl concentration of 10^{-3} M.

The variations in the dimensionless velocity profile at $z = b/2$ with different δ, ζ, K and β values are presented in Fig. 3. As shown in Fig. 3(a), an increase in δ leads to a higher velocity within the inner region of the microchannel while causing a decrease in velocity within the outer region. That is to say, increasing δ leads to a notable increase in the difference between the axial velocity of the inner and outer regions. A possible reason for this is as follows. An increase in δ leads to an increase in the axial electric force within the

inner region, as demonstrated by Eqs. (11) and (13), resulting in increased velocity in the inner region. However, the axial electric force in the outer region decreases as δ increases, resulting in a decrease in velocity in that area. The study conducted by Nekoubin[26] reported similar behavior for an EOF in a curved rectangular microchannel under no-slip conditions. Figure 3(b) shows that the velocity increases with the absolute value of zeta potential ζ. This is because a higher ζ indicates greater net charge in the fluid, resulting in enhanced electric body force and, consequently, increased velocity. As shown in Fig. 3(c), with increasing K the velocity gradient near the wall increases. This is because a larger electrokinetic width K corresponds to a thinner electric double layer, which amplifies the velocity gradient in the region. Moreover, the velocity increases with K in Fig. 3(c), which can be attributed to the amplification of the electric body force for larger values of K. Figure 3(d) describes the influence of the slip length β on velocity. The velocity increases with increasing slip length β, as depicted in Fig. 3(d), due to the reduced resistance at the channel wall for a longer slip length. The most significant observation in Fig. 3(d) is that an increase in slip length β leads to a more pronounced velocity enhancement near the inner wall of the curved channel, while the magnitude of this increase in velocity diminishes towards the outer wall region because of the smaller electric force in the outer region. The nonuniform velocity distribution in curved channels confers advantages for heat transfer, and the magnitude of these benefits increases as the velocity gradient increases.

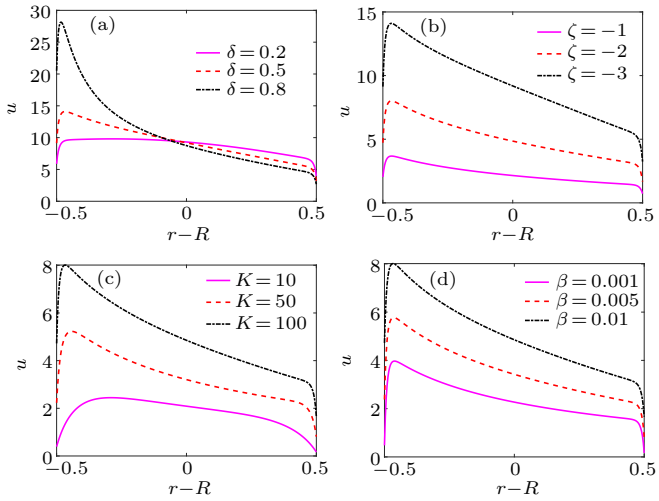


Fig. 3. Dimensionless velocity profile at $z = b/2$ for (a) different δ values for $\beta = 0.01$, $\zeta = -3$ and $K = 100$; (b) different ζ values for $\delta = 0.5$, $\beta = 0.01$ and $K = 100$; (c) different K values for $\delta = 0.5$, $\beta = 0.01$ and $\zeta = -2$; and (d) different β values for $\delta = 0.5$, $\zeta = -2$ and $K = 100$.

Contour plots of the solutions for the dimensionless velocity u are presented in Fig. 4 for different aspect ratios A_R at $\delta = 1/3$, $\beta = 0.01$ and $K = 10$. As shown in Fig. 4, the maximum velocity shifts towards the inner wall, with this shift becoming more pronounced as A_R increases. This is due to the greater electric force E^* in the inner region, which arises from the shorter arc length within this area. The investigation conducted by Norouzi *et al.*[53] of pressure-driven flow in a curved rectangular microchannel demonstrated a similar maximum velocity shift phenomenon.

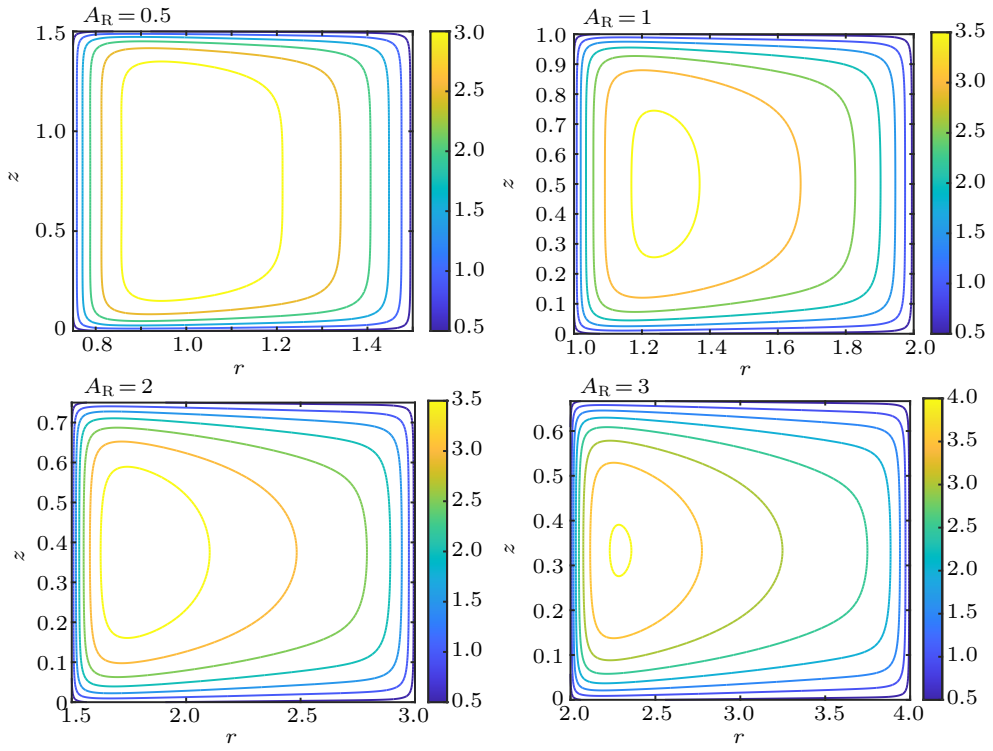


Fig. 4. Contours of dimensionless velocity u for different A_R at $\delta = 1/3$, $\beta = 0.01$ and $K = 10$.

Figure 5 illustrates the impact of slip length β on the dimensionless average velocity Q for different δ values at $\zeta = -3$ and $K = 100$. The dimensionless average velocity Q demonstrates a consistent increase as β increases, as illustrated in Fig. 5. This is because the velocity increases everywhere with increasing β, as illustrated in Fig. 3. Moreover, the results depicted in Fig. 5 reveal an intriguing observation: the average velocity Q exhibits a positive correlation with the parameter δ, indicating an upward trend. The reason for this can be found in Fig. 3, which shows that an increase in δ leads to a decrease in velocity in the outer region, while simultaneously causing a greater increase in velocity within the inner region. The combined influence of these two factors ultimately enhances the mean velocity Q. These results demonstrate that a curved hydrophobic microchannel with a larger curvature ratio δ is more suitable for achieving an increased EOF rate.

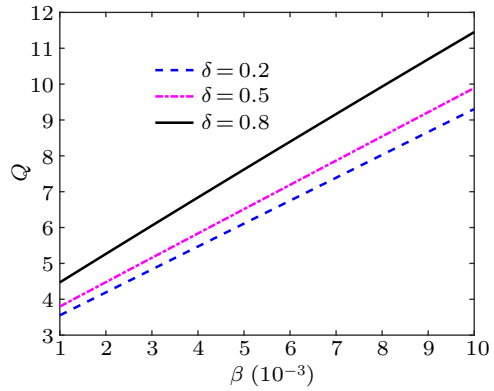


Fig. 5. Variations of dimensionless average velocity Q with β for different δ at $\zeta = -3$ and $K = 100$.

4. Conclusions

In this study, creeping Dean EOF through a curved rectangular microchannel with slip boundary conditions was investigated. The results reveal that increasing the curvature ratio δ leads to a higher velocity within the inner region of the curved channel while simultaneously causing a decrease in the velocity in the outer region. The combined influence of these two factors ultimately results in an enhanced average velocity. Also, consideration of the boundary slip condition results in increase in the velocity, which becomes increasingly significant as the curvature ratio δ and slip length β increase. Finally, the maximum velocity shifts towards the inner wall of the curved microchannel, with the shift becoming more pronounced as the aspect ratio A_{R} is increased.

The obtained results suggest that the velocity distribution of EOF in a curved hydrophobic microchannel is non-uniform, particularly for channels with large δ or A_{R} values. This non-uniformity, in conjunction with the high average velocity, may endow curved hydrophobic microchannels with certain advantages in terms of heat transfer.

These conclusions establish a fundamental basis for the design of a high-efficiency electroosmotic pump by taking into account the influence of the curvature and slip effects.

Appendix A

Partial differential equations (Eqs. (2) and (11)) with boundary conditions (Eqs. (3) and (12)) were solved in a rectangular domain $[r_{\mathrm{i}}, r_{\mathrm{o}}] \times [0, b]$ in the plane using the finite-difference method. In the horizontal direction we take $M = m-1$ steps, whereas in the vertical direction we take $N = n-1$ steps. Thus, the mesh sizes in the horizontal and vertical directions can be expressed as $h = (r_{\mathrm{o}} - r_{\mathrm{i}})/M$ and $k = (b-0)/N$. The centered-difference formula was used to compute the first and second derivatives. Thus, Eq. (2) has the following difference form:[47]

$$\begin{aligned}&\frac{\psi(r-h,z)-2\psi(r,z)+\psi(r+h,z)}{h^2}\\&+\frac{1}{r}\frac{\psi(r+h,z)-\psi(r-h,z)}{2h}+O(h^2)\\&+\frac{\psi(r,z-k)-2\psi(r,z)+\psi(r,z+k)}{k^2}\\&+O(k^2)+K^2\sinh[\psi(r,z)]=0.\end{aligned}\tag{A1}$$

The grid points are $(r(i), z(j))$, where $r(i) = r_{\mathrm{i}} + (i-1)h$ for $1 \le i \le m$ and $z(j) = (j-1)k$ for $1 \le j \le n$. By neglecting the higher-order infinite terms in Eq. (A1) and approximating the solution as $w_{i,j} \approx \Psi(r(i), z(j))$, we obtain

$$\begin{aligned}&\frac{w_{i-1,j}-2w_{i,j}+w_{i+1,j}}{h^2}+\frac{1}{r(i)}\frac{w_{i+1,j}-w_{i-1,j}}{2h}\\&+\frac{w_{i,j-1}-2w_{i,j}+w_{i,j+1}}{k^2}+K^2\sinh(w_{i,j})=0\end{aligned}\tag{A2}$$

for $2 \le i \le m-1$ and $2 \le j \le n-1$. The boundary points are governed by the following equations:

$$w_{i,j} = \zeta \quad \text{for} \quad i = 1, \quad 1 \le j \le n, \tag{A3}$$

$$w_{i,j} = \zeta \quad \text{for} \quad i = m, \quad 1 \le j \le n, \tag{A4}$$

$$w_{i,j} = \zeta \quad \text{for} \quad j = 1, \quad 1 \le i \le m, \tag{A5}$$

$$w_{i,j} = \zeta \quad \text{for} \quad j = n, \quad 1 \le i \le m. \tag{A6}$$

The solutions to Eqs. (A2) and (A3)–(A6) can be obtained by applying the multivariate Newton method.[25,47] The difference form of Eq. (11) can be expressed as follows:

$$\begin{aligned}&\frac{u(r-h,z)-2u(r,z)+u(r+h,z)}{h^2}\\&+\frac{1}{r}\frac{u(r+h,z)-u(r-h,z)}{2h}-\frac{u(r,z)}{r^2}+O(h^2)\\&+\frac{u(r,z-k)-2u(r,z)+u(r,z+k)}{k^2}+O(k^2)\\&=K^2\sinh[\psi(r,z)]\frac{R}{r}.\end{aligned}\tag{A7}$$

By approximating the solution as $v_{i,j} \approx u(r(i), z(j))$, we obtain

$$\frac{v_{i-1,j}-2v_{i,j}+v_{i+1,j}}{h^2}+\frac{1}{r(i)}\frac{v_{i+1,j}-v_{i-1,j}}{2h}-\frac{v_{i,j}}{r(i)^2}$$

$$+\frac{v_{i,j-1}-2v_{i,j}+v_{i,j+1}}{k^2}$$
$$=K^2\sinh(w_{i,j})\frac{R}{r(i)}, \tag{A8}$$

for $1\le i\le m$ and $1\le j\le n$. Examining Eq. (A8), it is evident that certain terms are virtual points, such as the term $v_{i-1,j}$ for $i=1$. The values of these virtual points were derived by considering the boundary equations, which are expressed as

$$v_{i,j}=\beta\frac{v_{i+1,j}-v_{i-1,j}}{2h} \quad \text{for } i=1,\ 1\le j\le n, \tag{A9}$$
$$v_{i,j}=-\beta\frac{v_{i+1,j}-v_{i-1,j}}{2h} \quad \text{for } i=m,\ 1\le j\le n, \tag{A10}$$
$$v_{i,j}=\beta\frac{v_{i,j+1}-v_{i,j-1}}{2k} \quad \text{for } j=1,\ 1\le i\le m, \tag{A11}$$
$$v_{i,j}=-\beta\frac{v_{i,j+1}-v_{i,j-1}}{2k} \quad \text{for } j=n,\ 1\le i\le m. \tag{A12}$$

Acknowledgements

Project supported by the Natural Science Foundation of Inner Mongolia of China (Grant No. 2021BS01008), the Program for Innovative Research Team in Universities of Inner Mongolia Autonomous Region (Grant No. NMGIRT2323), and the Scientific Research Funding Project for introduced high level talents of IMNU (Grant No. 2020YJRC014). I would like to thank Editage (www.editage.cn) for English language editing.

References

[1] Engler M, Kockmann N, Kiefer T and Woias P 2004 *Chem. Eng. J.* **101** 315
[2] Manz1 A, Effenhauser C S, Burggraf N, Harrison D J, Seiler K and Fluri K 1994 *J. Micromech. Microeng.* **4** 257
[3] Yamamoto K, Ota N and Tanaka Y 2021 *Anal. Chem.* **93** 332
[4] Kleinstreuer C, Li J and Koo J 2008 *Int. J. Heat Mass Transf.* **51** 5590
[5] Tegenfeldt J O, Prinz C, Cao H, Huang R L, Austin R H, Chou S Y, Cox E C and Sturm J C 2004 *Anal. Bioanal. Chem.* **378** 1678
[6] Mala G M, Li D and Dale J D 1997 *Int. J. Heat Mass Transf.* **40** 3079
[7] Hu Y, Werner C and Li C 2003 *J. Fluids Eng.* **125** 871
[8] Yan B, Chen B, Xiong Y and Peng Z 2021 *Chin. Phys. B* **30** 114701
[9] Yang C H and Jian Y J 2020 *Chin. Phys. B* **29** 114101
[10] Wiedemann G 1852 *Poggendorfs Annalen* **87** 321
[11] Yang R J, Fu L M and Lin Y C 2001 *J. Colloid Interf. Sci.* **239** 98
[12] Sadr R, Yoda M, Zheng Z and Conlisk Z 2004 *J. Fluid mech.* **506** 357
[13] Wang C Y, Liu Y H and Chang C C 2008 *Phys. Fluids* **20** 063105
[14] Jian Y J, Yang L G and Liu Q S 2010 *Phys. Fluids* **22** 042001
[15] Jiang F, Drese K S, Hardt S, Küpper M and Schönfeld F 2004 *AIChE J.* **50** 2297
[16] Ookawara S, Higashi R, Street D and Ogawa K 2004 *Chem. Eng. J.* **101** 171
[17] Zourob M, Mohr S, Mayes S, Macaskill A, Pérez-Moral N, Fielden P R and Goddard N J 2006 *Lab Chip* **6** 296
[18] Kockmann N, Engler M, Haller D and Woias P 2005 *Heat Transf. Eng.* **26** 71
[19] Schönfeld F and Hardt S 2004 *AIChE J.* **50** 771
[20] Luo W J 2004 *J. Colloid Interf. Sci.* **278** 497
[21] Luo W J, Pan Y J and Yang R J 2005 *J. Micromech. Microeng.* **15** 463
[22] Chen J K, Luo W J and Yang R J 2006 *Jpn. J. Appl. Phys.* **45** 7983
[23] Lu D C, Noreen S, Waheed S and Tripathi D 2022 *J. Mech. Med. Biol.* **22** 2250030
[24] Salahuddin T, Kousar I, and Khan M 2022 *Mater. Sci. Eng. B* **284** 115886
[25] Liu Y, Xing J and Jian Y 2022 *Int. Commu. Heat Mass Transf.* **139** 106501
[26] Nekoubin N 2018 *J. Non-Newton. Fluid Mech.* **260** 54
[27] Narla V K and Tripathi D 2019 *Microvasc. Res.* **123** 25
[28] Kolsi L, Javid K, Safra I, Ghachem K, Khan S U and Albalawi H 2023 *Case Stud. Therm. Eng.* **49** 103201
[29] Khan A A, Zahra B, Ellahi R, Sait S M 2023 *Symmetry* **15** 889
[30] Si X, Lei X, Xu B, Li B, Zhu J and Cao L 2023 *Phys. Fluids* **35** 032005
[31] Yang X, Zhao M, Wang S and Xiao Y 2023 *Phys. Fluids* **35** 053106
[32] Choi C H, Ulmanella U, Kim J, Ho C M and Kim C J 2006 *Phys. Fluids* **18** 087105
[33] Goswami P, Kumar Mondal P, Dutta S and Chakraborty S 2015 *Electrophoresis* **36** 703
[34] Shit G C, Mondal A, Sinha A and Kundu P K 2016 *Colloids Surf. A: Physicochem. Eng. Aspects* **506** 535
[35] Majhi M, Nayak A K and Sahoo S 2023 *Phys. Fluids* **35** 012014
[36] Sujith T, Mehta S K and Pati S 2023 *J. Therm. Anal. Calorim.* **148** 489
[37] Banerjee D, Mehta S K, Pati S and Biswas P 2021 *Int. J. Heat Mass Transf.* **181** 121989
[38] Banerjee D, Pati S and Biswas P 2023 *Appl. Math. Mech.* **44** 1007
[39] Vasista K N, Mehta S K and Pati S 2022 *Chem. Eng. Process.* **176** 108940
[40] Vasista K N, Mehta S K, Pati S and Sarkar S 2021 *Phys. Fluids* **33** 123110
[41] Nath A J, Roy P, Banerjee D, Pati S, Randive P R and Biswas P 2023 *J. Fluids Eng.* **145** 014501
[42] Mahanta K, Panda S, Banerjee D, Pati S and Biswas P 2022 *Phys. Scr.* **98** 015212
[43] Xie Z 2022 *Colloids Surf. A: Phys. Eng. Aspects* **651** 129710
[44] Banerjee D, Pati S and Biswas P 2022 *Phy. Fluids* **34** 032013
[45] Liu Y, Jian Y and Yang C 2020 *Energy* **198** 117401
[46] Deng S, Li M, Yang Y and Xiao T 2021 *Appl. Therm. Eng.* **196** 117314
[47] Sauer T 2013 *Numerical Analysis*, 2nd edn. (New York: Pearson Education Inc) pp. 375–405
[48] Jian Y 2015 *Int. J. Heat Mass Transf.* **89** 193
[49] Xie Z Y and Jian Y J 2017 *Energy* **139** 1080
[50] Liu Y, Jian Y and Tan W 2018 *Int. J. Heat Mass Transf.* **127** 901
[51] Xing J and Liu Y 2023 *Phys. Scr.* **98** 025202
[52] Wang C, Wong T N, Yang C and Ooi K T 2007 *Int. J. Heat Mass Transf.* **50** 3115
[53] Norouzi M, Zare Vamerzani B, Davoodi M, Biglari N and Shahmardan M M 2015 *Rheol. Acta* **54** 391